Crystal structures of reduced, oxidized, and mutated human thioredoxins: evidence for a regulatory homodimer

Andrzej Weichsel[1], John R Gasdaska[2], Garth Powis[2] and William R Montfort[1]*

Background: Human thioredoxin reduces the disulfide bonds of numerous proteins *in vitro*, and can activate transcription factors such as NFκB *in vivo*. Thioredoxin can also act as a growth factor, and is overexpressed and secreted in certain tumor cells.

Results: Crystal structures were determined for reduced and oxidized wild type human thioredoxin (at 1.7 and 2.1 Å nominal resolution, respectively), and for reduced mutant proteins Cys73→Ser and Cys32→Ser/Cys35→Ser (at 1.65 and 1.8 Å, respectively). Surprisingly, thioredoxin is dimeric in all four structures; the dimer is linked through a disulfide bond between Cys73 of each monomer, except in Cys73→Ser where a hydrogen bond occurs. The thioredoxin active site is blocked by dimer formation. Conformational changes in the active site and dimer interface accompany oxidation of the active-site cysteines, Cys32 and Cys35.

Conclusions: It has been suggested that a reduced pK_a in the first cysteine (Cys32 in human thioredoxin) of the active-site sequence is important for modulation of the redox potential in thioredoxin. A hydrogen bond between the sulfhydryls of Cys32 and Cys35 may reduce the pK_a of Cys32 and this pK_a depression probably results in increased nucleophilicity of the Cys32 thiolate group. This nucleophilicity, in turn, is thought to be necessary for the role of thioredoxin in disulfide-bond reduction. The physiological role, if any, of thioredoxin dimer formation remains unknown. It is possible that dimerization may provide a mechanism for regulation of the protein, or a means of sensing oxidative stress.

Addresses: [1]Department of Biochemistry, University of Arizona, Tucson, AZ 85721, USA and [2]Arizona Cancer Center, University of Arizona Health Sciences Center, Tucson, AZ 85724, USA.

*Corresponding author.
E-mail: montfort@biosci.arizona.edu

Key words: dimer, mutant, oxidation, thioredoxin, X-ray crystallography

Received: 5 Feb 1996
Revisions requested: 27 Feb 1996
Revisions received: 19 Apr 1996
Accepted: 25 Apr 1996

Structure 15 June 1996, 4:735–751

Introduction

Thioredoxin is a small (~12 kDa) protein found in all living cells. The protein uses the conserved sequence Trp–Cys–Gly–Pro–Cys to either reduce disulfide bonds or oxidize sulfhydryls in a variety of proteins, both intracellularly and extracellularly. The first characterized role for the protein was as part of a system that shuttles hydrogen from NADPH, through thioredoxin reductase and thioredoxin, to the oxidized form of the essential enzyme ribonucleotide reductase, resulting in a reduced disulfide bond in this latter reductase (reviewed in [1–3]). During this sequence, cysteines in the thioredoxin active site undergo both disulfide bond reduction and oxidation, and form transient mixed disulfide bonds with the two reductases. More recently, thioredoxin and proteins with thioredoxin-like domains (reviewed in [4]) have been implicated in several seemingly unrelated processes: transcription factor modulation (of NFκB [5], the glucocorticoid receptor [6], and AP-1 through Ref-1 [7]); protein folding (by protein disulfide isomerase [8] and DsbA [9]); cell growth stimulation (as a domain in the gonadotropic hormones [10] and as an exported thioredoxin, summarized in [11]); cell growth inhibition (by interferon-γ [12]); in pregnancy (as a component of the early pregnancy factor [13]); and in reduction of sulfenic and sulfinic acids [14]. This broad specificity for thioredoxin and related proteins has made it difficult to distinguish true physiological partners for the protein from *in vitro* artifacts.

Two functional aspects of thioredoxin and related proteins have recently received considerable attention. The first concerns the means by which the redox potential is modulated among the thioredoxin family of proteins. All thioredoxin-like proteins contain the active-site sequence CXXC, and all apparently have depressed pK_as for the first cysteine in this sequence. For example, Cys32 in human thioredoxin has an estimated pK_a of 6.3 [15], and Cys30 of DsbA, a disulfide oxidoreductase found in the *E. coli* periplasm, has an estimated pK_a of 3.5 [16]. The unperturbed pK_a of cysteine is about 8.7. (Numbering used throughout is for human thioredoxin, starting from the N-terminal methionine. Residues from the second monomer of the thioredoxin homodimer are designated with a prime (′), as in Cys73′.) The oxidative power among these proteins is also variable, with thioredoxin being more reducing than, for example DsbA. This factor relates to function: thioredoxin helps maintain the reducing environment of the *E. coli* cytosol, and DsbA the oxidizing environment of the *E. coli* periplasm. Considerable effort has recently been concentrated on understanding how the

oxidative power of proteins in the thioredoxin family is related to the reduced pK_a of the first active-site cysteine, and how the active-site environment modulates this pK_a. Approaches to these questions have included structural [1,4], mutagenic [17,18], and modeling [19,20] studies, and it is clear that both the cysteine pK_a and the thioredoxin redox potential can be modulated by simply altering the residues in the X positions of the CXXC amino-acid segment. However, the mechanism by which the cysteine pK_a is lowered remains unclear.

A second area of recent interest is the role of thioredoxin as an extracellular growth factor in mammalian tissues. Thioredoxin has been identified as the growth factor secreted by virus-transformed leukemic cell lines (referred to as adult T-cell derived leukemic factor or ADF [21]), and is overexpressed in certain tumors and tumor-derived cell lines [22–24]. The protein can be secreted by cells [25–27] through an unusual leaderless pathway [26]. Exogenously added human thioredoxin, but not *E. coli* thioredoxin, is capable of stimulating growth in a number of solid-tumor derived cell lines in the absence of serum, conditions under which many growth factors are incapable of working [11]. These findings suggest that thioredoxin may function as a growth factor for some forms of cancer. Although the mechanism by which thioredoxin works in this regard is not yet clear, it requires a functional thioredoxin active site [28], but apparently does not require a stable thioredoxin–receptor complex to be formed [11]. It is possible that extracellular thioredoxin functions by enhancing the activity of endogenously produced growth factors [11]. Cancer cells transfected with wild-type thioredoxin show increased anchorage-independent growth while a redox-inactive mutant thioredoxin acts in a dominant-negative manner to inhibit anchorage-independent growth (GP and JRG, unpublished observations). A series of imidazolyl disulfide containing compounds that inhibit thioredoxin and thioredoxin reductase can also prevent cell-growth stimulation by thioredoxin in cell culture [29,30]. Thus, human thioredoxin may provide an excellent target for rational drug design.

Extensive structural data exist for thioredoxin. The crystal structures of oxidized thioredoxin from *E. coli* [31,32] and the cyanobacteria *Anabaena* [33] have been determined, as well as the oxidized and reduced solution structures of thioredoxin from *E. coli* [34] and a mutated form of the human protein [35]. The NMR structure of the same mutated human thioredoxin has also been determined in a disulfide-linked complex with a peptide from the transcription factor NFκB [36]. The human protein used in the NMR studies is mutated at four sites: three non-active-site surface cysteines are replaced by alanine (Cys62→Ala, Cys69→Ala, Cys73→Ala), and Met74 by threonine (Met74→Thr). The cysteines were changed to eliminate difficulties with the formation of interchain disulfide bonds [35,37], and the Met74→Thr mutation is apparently a cloning artifact [21,23,38–40]. In all of these structures thioredoxin is a compact globular protein with a five-stranded β sheet surrounded by four α helices. The conserved active site amino acids Trp–Cys–Gly–Pro–Cys link the second β strand to the second α helix, and form the first turn of the second helix. Differences in the position and hydrogen bonding of these amino acids in the human and *E. coli* structures has contributed to the uncertainty as to which components of the thioredoxin active site are necessary for a reduced cysteine pK_a [35,41].

Here we report the crystal structure of reduced wild-type human thioredoxin (Trx-red), the first such crystal structure for any thioredoxin, and only the second for any protein in the thioredoxin family [42]. We also report the structure of the oxidized human protein (Trx-ox), and the structures of two mutant forms of the protein (Cys73→Ser, C73S; Cys32→Ser/Cys35→Ser, C32S/C35S) designed to probe the role of disulfide bond formation in thioredoxin catalytic activity and oligomerization. In all of these structures an unexpected dimeric form of human thioredoxin was revealed, as well as a redox-dependent conformational change in the active site and an unusual thiol–thiol hydrogen bond that provides an explanation for the depressed pK_a of the first cysteine in the active site, Cys32.

Results and discussion

Structure determinations

Crystals of wild-type human thioredoxin were obtained from a 50% 2-methyl-2,4-pentanediol (MPD) solution buffered at pH 3.8, and diffracted beyond 1.7 Å nominal resolution. The reductant dithiothreitol (DDT; 1–10 mM) was required for crystal formation; the crystals used for data measurement were grown in the presence of 5 mM DTT. The structure was determined by molecular replacement using the NMR structure of the Met74→Thr variant of human thioredoxin as a starting model (PDB entry 3TRX [43]). The higher resolution human quadruple mutant (hQM-Trx) NMR model described in the Introduction was not available at the outset of the present study, but has been used in the comparisons below. The single and quadruple mutant thioredoxin NMR models are not substantially different [35]. Residue 74 was left as a threonine in the initial search model, and provided a convenient internal check on the progress of the molecular replacement structure determination.

Trx-red was refined to a crystallographic R factor of 0.21 at 1.7 Å resolution (Table 1). The crystal structure was very similar to the solution structure of the quadruple mutant protein except for two striking features: the active-site loop containing Cys32 and Cys35 had shifted by approximately 4 Å and the protein crystallized as a disulfide-linked dimer

Table 1

Data collection and refinement parameters.

Crystal	Trx-red	Trx-ox	C32S/ C35S	C73S
Space group	C2	C2	C2	C2
a (Å)	67.9	67.8	67.8	67.8
b	26.5	26.4	26.4	26.3
c	51.7	51.8	51.6	51.5
β (°)	95.2	94.9	95.1	95.0
Data collection				
Resolution (Å)	15–1.7	15–2.1	15–1.8	7–1.65
Total reflections	19 412	8894	23 947	22 700
Unique reflections	9477	4440	7917	9449
Completeness (%)				
Overall	92	80	91	85
Outermost data shell	78	71	77	69
R-sym	0.047	0.049	0.044	0.064
Mean I/σ(I)				
Overall	44.9	40.4	52.0	28.8
Outermost data shell	7.0	12.7	7.9	4.4
R-iso	–	0.20	0.14	0.13
Refinement				
R-cryst	0.21	0.22	0.21	0.21
R-free	0.24	0.33	0.26	0.24
Rms deviation in:				
Bond lengths (Å)	0.015	0.016	0.016	0.016
Bond angles (°)	2.8	2.8	2.7	2.6
Number of solvent molecules	45	36	49	58
Average B factor	17	19	18	20

Trx-red, wild-type thioredoxin with reduced sulfhydryls in the active site; Trx-ox, wild-type thioredoxin with oxidized sulfhydryls in the active site; C73S, mutated thioredoxin with Cys73 replaced by serine; C32S/C35S, doubly mutated thioredoxin with Cys32 and Cys35 changed to serine; R-sym, R-factor for symmetry related intensities; R-iso, R-factor between Trx-red amplitudes and amplitudes from the other crystals; R-cryst, crystallographic R-factor; R-free, R-factor for a randomly selected 10% of reflections not included in the refinement.

connected through Cys73 from each monomer. The two active-site cysteines were in the reduced form, as shown in the $2F_o–F_c$ electron density map in Figure 1a. The positions for all 105 amino acids are clear in the current electron-density map except for the Cα and Cβ atoms of Trp31, which are apparently disordered (this is not the case for the oxidized structure, discussed below), and the N-terminal methionine, which is either poorly ordered in the crystal (it makes only one intramolecular and no intermolecular contacts), or not present in all copies of the protein. The N-terminal methionine may be cleaved from human thioredoxin *in vivo* [3,44,45]. The side chains of Asp20, His43 and Ser90 occupy two positions in the crystal and have been refined as such.

Crystals of Trx-ox, C32S/C35S, and C73S were isomorphous with crystals of Trx-red, and the structures of these proteins were determined through manual rebuilding of the Trx-red structure into difference, unbiased omit (where phase bias toward the atoms to be fitted has been removed), and $2F_o–F_c$ electron-density maps, alternated with cycles of least squares refinement. Crystals of oxidized thioredoxin were obtained by allowing the crystals of the reduced protein to slowly oxidize over a two month period (we have been unable to obtain crystals in the absence of reductant). Numerous local changes occurred in the protein on oxidation resulting in reduced diffraction and a lower quality model than for the other three structures (discussed below). The C32S/C35S and C73S structures were essentially identical to Trx-red, except in the active-site and dimer-interface regions. All cysteines not involved in disulfide bonds appeared fully reduced in all four structures, as judged by $F_o–F_c$ and omit electron-density maps, and temperature factors for the sulfhydryls were similar to those for nearby atoms. Maintaining reduced cysteines was aided by relatively fast experimental parameters: crystal growth and data measurement were completed in less than a week for each of the Trx-red, C73S, and C32S/C35S structure determinations. Difference electron-density maps between Trx-red and each of Trx-ox, C32S/C35S, and C73S are shown in Figures 1 and 2.

Dimeric human thioredoxin

Surprisingly, thioredoxin is dimeric in all four structures determined in the present work. The crystals contain a monomer in the asymmetric unit and the two monomers of each dimer are related through the crystallographic twofold rotation axis. Thioredoxin is thought to function as a monomer in redox reactions. An inactive dimeric form of human thioredoxin has previously been noted, leading to the suggestion that dimer formation may function in a regulatory capacity [37,46]. The dimer interface of Trx-red consists of three components: an approximately 1100 Å^2 (550 Å^2 per monomer) largely hydrophobic patch; five hydrogen bonds; and the Cys73–Cys73′ disulfide bond. Oligomeric organization in crystallized proteins is not uncommon (see, for example, the packing in *E. coli* thioredoxin crystals [31]). Therefore a logical question to ask at this stage is whether the dimer found in these crystals represents a normal state for the protein. Discussed below are several lines of evidence that suggest the answer to this question is yes.

Electron density for the Cys73–Cys73′ disulfide bond is shown in Figure 2a, and the thioredoxin dimer interface is shown in Figures 3–5. The disulfide bond lies directly on the dimer twofold axis, on one side of a short, two-stranded β sheet comprising residues 72–74 from each monomer, and is solvent exposed (Fig. 3,4b). The bond is apparently quite stable in the dimer as it occurs despite the presence of 5 mM DTT in the crystallization drop, a concentration sufficient to keep the active-site sulfhydryls in the reduced state. The reason for this stability is not clear but it is probably due in part to the perfect orientation for disulfide-bond formation of the two sulfhydryls in the dimer, and the sterically restricted space for the two groups in the dimer.

Figure 1

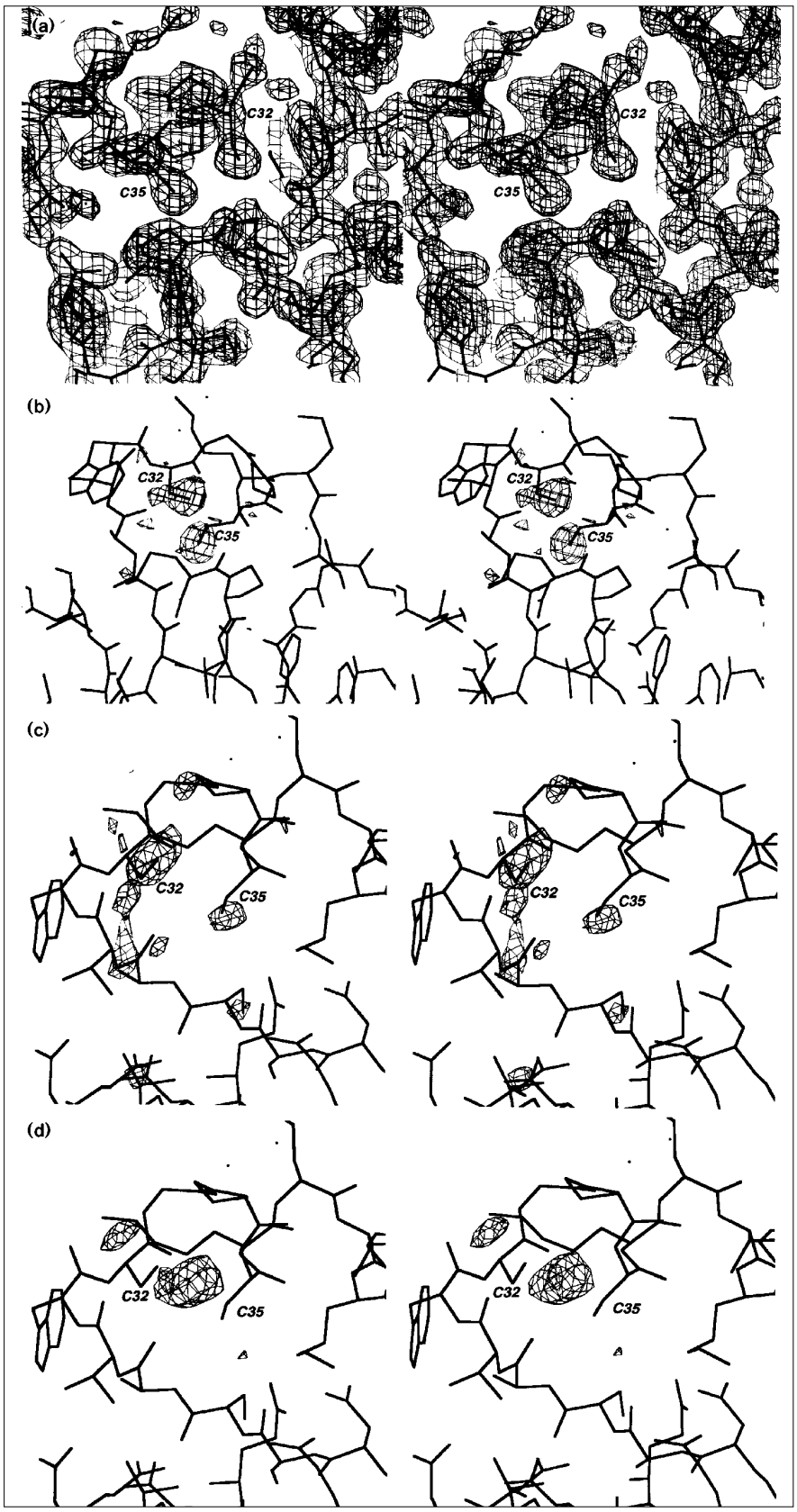

Stereoviews of active site electron density (Trx-red) and difference electron density (C32S/C35S and Trx-ox). (a) $2F_o–F_c$ electron-density map for Cys32 and Cys35 in the Trx-red structure (contoured at 1.0σ above the mean value for the map). (b) Difference electron density map between Trx-red and C32S/C35S, showing Cys32 and Cys35. Only positive electron density is shown (contoured at 2.7σ). (c) Difference electron density map between Trx-red and Trx-ox, showing Cys32 and Cys35. Positive electron density contoured at 2.7σ is shown. (d) Same map as in (c), showing negative electron density contoured at 2.7σ. (Figure produced with FRODO [71,72].)

Figure 2

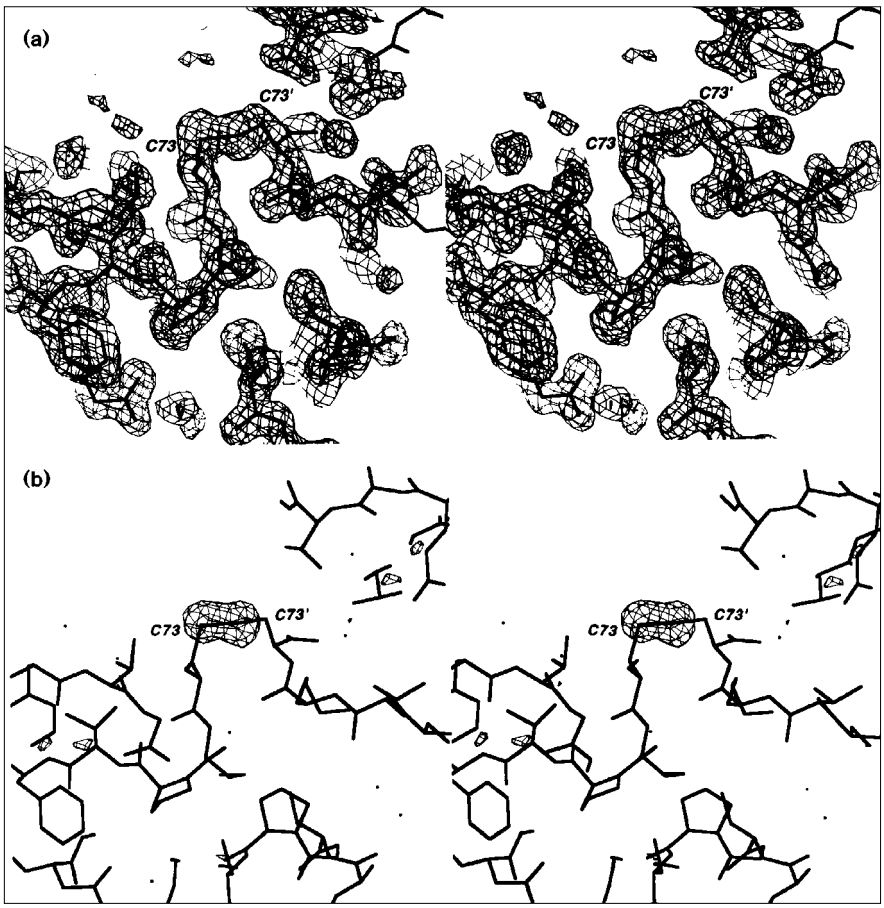

Stereoviews of electron density for Cys73 and Ser73. (a) $2F_o–F_c$ electron density map for the C73–C73′ disulfide bond in Trx-red (contoured at 1.0σ above the mean value for the map). (b) Difference electron density map between Trx-red and C73S for residue 73. Only positive electron density is shown (contoured at 2.7σ). (Figure produced with FRODO [71,72].)

The dimer interface is composed of 24 amino acids (12 from each monomer, Figs 4,6), and covers about 10% of the 5750 Å^2 solvent-accessible surface of the monomer. The majority of the contacts between monomers are hydrophobic. Two hydrophobic patches, consisting mostly of residues Trp31, Val59, Ala66, and Met74 from each monomer, fit together to completely bury all eight side chains. The resulting interface contains no intervening solvent molecules, and is sufficiently closely packed that no gaps large enough to accommodate a water molecule are present. However, a small cavity does occur in the interface between Trp31 from each monomer. This cavity allows the two tryptophans to move toward one another upon disulfide-bond formation in the active site (discussed below). Four groups which can form hydrogen bonds, the carbonyl of Val59 and the nitrogen of the Trp31 indole ring from each monomer, are buried and left unsatisfied in the dimer.

Five hydrogen bonds are formed in the dimer interface. Two of these result from the short interfacial antiparallel β sheet: the carbonyl of Lys72 from each monomer hydrogen bonds to the nitrogen of Met74 on the opposite monomer (2.8 Å). Two more result from the side chains of Ser67 hydrogen bonding to the carbonyls of Trp31 in the opposite monomers (3.0 Å). The fifth occurs between the side chains of Asp60 from each monomer (3.2 Å). Such a hydrogen bond, which requires a shared proton between two carboxylates, is common at the crystallization pH of 3.8, but to occur at neutral pH it would require a pK_a elevated above the normal value of about 3.9. Whether this hydrogen bond exists at neutral pH is not yet known, but occurrences of appropriately elevated pK_as for aspartate are well documented (see, for example, [47–49]). One factor which could serve to elevate the pK_a of Asp60 in dimeric thioredoxin is its proximity to Asp58 (Fig. 5a), which is more solvent exposed and likely to have a lower pK_a than Asp60. Alternatively, Asp60 and Asp60′ might swing away from one another in the anionic state, as they lie on the edge of the dimer interface (Fig. 3b). In oxidized thioredoxin, the Asp60–Asp60′ hydrogen bond is replaced with hydrogen bonds to Trp31 and Trp31′ (discussed below).

The residues in the dimer interface are poorly conserved among thioredoxins from 39 widely divergent species [33], but highly conserved among eight vertebrate species

Figure 3

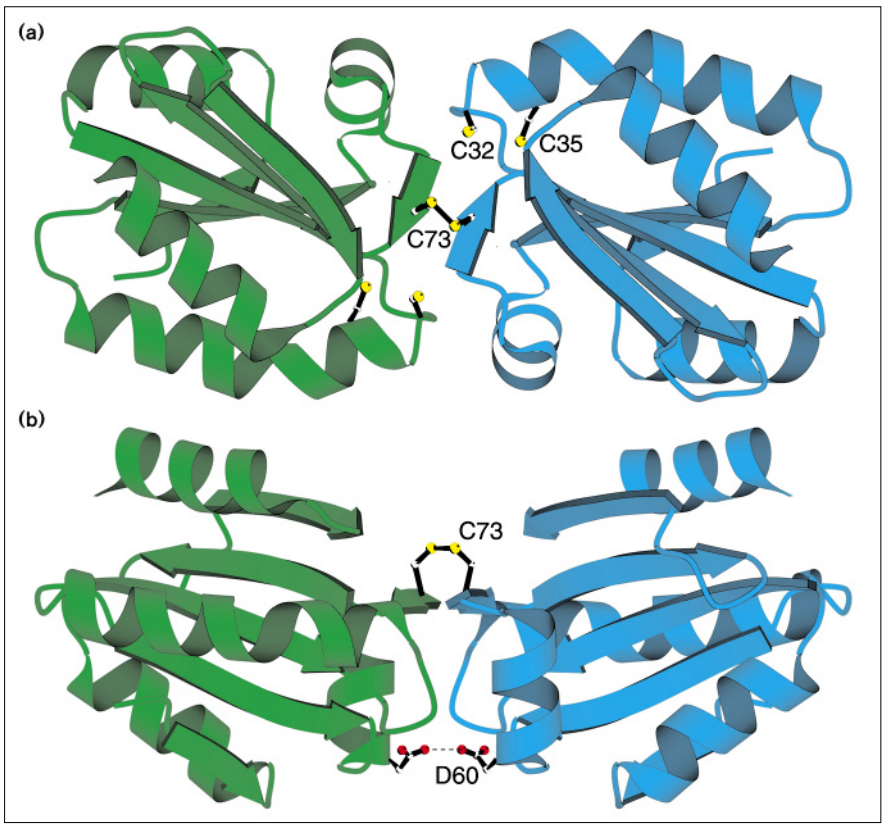

Ribbon drawing of the Trx dimer. (a) A view parallel to the twofold rotation axis; (b) view is perpendicular to the twofold axis. Ball-and-stick representations for residues Cys32, Cys35, and Cys73 are shown in (a), and Asp60 and Cys73 in (b). (Figure drawn with MOLSCRIPT [75].)

(Fig. 6). Overall, vertebrate thioredoxins are 62% identical, and 10 out of 12 amino acids in the dimer interface are invariant (83%). The two variable residues are Gln63 and Ser67. Gln63 forms van der Waals contacts with Trp31 and Thr30 of the opposite monomer, contacts which could still form in rabbit thioredoxin, in which residue 63 is a lysine (the amino group of the lysine would be solvent accessible in the rabbit dimer, as the amide of the Gln63 is in the human dimer). The change of Ser67 to alanine, which occurs in thioredoxins from several species, would result in the loss of a hydrogen bond in the dimer interface, however the exposed hydrogen bonding partner (carbonyl 31) would be solvent accessible. The conservation of the dimer interface amino acids suggests dimeric thioredoxin may be a recent occurrence, possibly evolving in response to the specific needs of higher animals, or to spread redox functions to new (extracellular?) compartments.

C73S

To begin investigating the features necessary for thioredoxin dimer formation, we determined the structure of the C73S mutant thioredoxin. This protein is fully functional in redox reactions ([37,50] and Gasdaska *et al.*, unpublished data), fully stimulates cell growth (Gasdaska *et al.*, unpublished data), shows a reduction in oxidation-related inactivation ([37], Gasdaska *et al.*, unpublished data), and is inactive as a component of the early pregnancy factor [50]. C73S crystallized under conditions nearly identical to those for the wild-type crystals, but grew more slowly, possibly due to a higher dimerization dissociation constant (discussed below).

Despite the loss of the dimer interface disulfide bond, C73S is dimeric in the crystal and is nearly identical to the wild-type protein except for a few small changes in the dimer interface. The introduced serines at position 73 are in a conformation very similar to that for the cysteines of the wild-type protein, and are connected through a hydrogen bond (3.2 Å, Fig. 5b). The dimer interface appears to have relaxed slightly in the mutant protein, especially near Trp31 where both main-chain and side-chain atoms have shifted by about 0.5 Å. This shift enlarged the small cavity between Trp31 from each monomer, allowing a poorly ordered water molecule into the dimer interface (Fig. 5b). This water lies on the crystallographic twofold axis and has been refined with an occupancy of 0.5 (B=28 $Å^2$). A similar shift in Trp31, but in the opposite direction, also occurs upon disulfide-bond formation in the active site (discussed below).

Figure 4

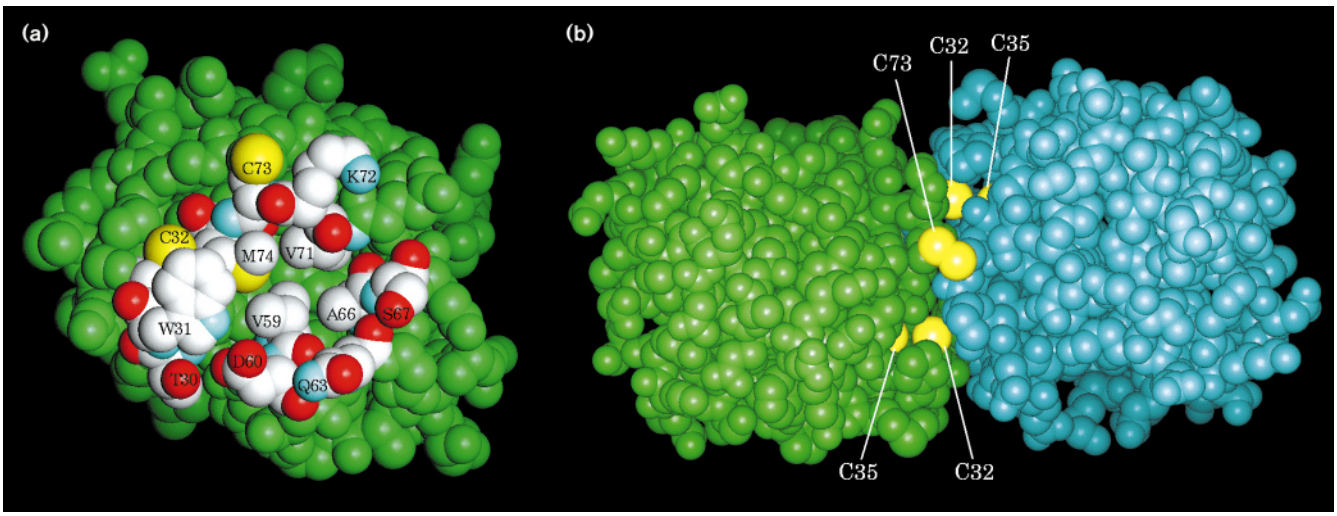

Space-filling model of thioredoxin. (a) Trx-red monomer with residues that make interchain contacts labeled and colored by atom type: carbon (white), oxygen (red), nitrogen (blue), and sulfur (yellow). (b) Trx-red dimer highlighting the positions of Cys32, Cys35, and the Cys73–Cys73′ disulfide bond. Cys32 and Cys35 are largely inaccessible in dimeric thioredoxin. (Figure produced with INSIGHT II [69].)

The similarity in the structures of the wild-type and C73S mutant proteins suggests that much of the thioredoxin dimerization energy is provided by the non-covalent interactions in the dimer interface, and does not simply depend on disulfide-bond formation.

Dimer formation in solution

As the data above suggest that the human thioredoxin dimer may play a physiological role, the conditions under which such a dimer can form is of interest. Some preliminary conclusions relating to this are discussed in this section.

It is clear that human thioredoxin can form covalently-linked dimers in solution [51], especially in the presence of a strong oxidant [37] or when stored at the moderately high concentration of 125 mM [11]. Covalently-linked dimer formation is greatly reduced or eliminated, depending on solution conditions, for the mutant thioredoxin C73S, which eliminates the dimer interface disulfide bond found in the present work ([37,50] and Gasdaska *et al.*, unpublished data). In our hands, wild-type thioredoxin stored for approximately two months at a concentration of 1 mM, pH 3.8, and 4°C, was almost entirely in the form of covalently-linked dimers, as judged by sodium dodecyl sulfate polyacrylamide gel electrophoresis (SDS-PAGE) in the absence of reductant, although a small percentage of monomeric and multimeric thioredoxin was also present (data not shown). The dimeric and multimeric bands disappear upon addition of fresh reductant. In contrast, C73S stored under similar conditions remained largely free of covalent dimers, although a small percentage of dimeric and multimeric thioredoxin was present (data not shown). It should be noted, however, that fresh reductant was necessary to obtain crystals of the wild-type protein.

The concentration dependence of dimer formation has not yet been fully characterized. Preliminary data for dimer formation of the C73S protein as estimated by difference UV spectroscopy suggest a dissociation constant of approximately 30 mM at pH 4.0, and a somewhat higher one at pH 7.5 where the charge repulsion between Asp60 from each monomer is likely to be greater (data not shown). The wild-type protein, with the potential for disulfide-bond formation across the dimer interface, might have a considerably lower dissociation constant. Thioredoxin concentrations in bovine tissue have been estimated to be 1 to 10 mM [52], but may be considerably higher in specific tissues where thioredoxin has been induced to higher levels of expression [22–24]. This suggests that thioredoxin concentrations may rise in certain tissues to a level where dimeric thioredoxin is apparently the favored form for the protein, and thus could play a regulatory role in thioredoxin function. Also, thioredoxin may pass through an oxidizing environment during export, and, under sufficiently high thioredoxin concentrations, dimer formation could protect the active site from oxidation.

Dimer formation was apparently not detected in the NMR structure determination, despite the use of 1.2 mM thioredoxin in the study [35]. A possible explanation is the presence of a threonine at amino acid 74, rather than a methionine as in the wild-type protein we used. Met74 is completely buried and tightly packed in the dimer interface (Fig. 5).

Figure 5

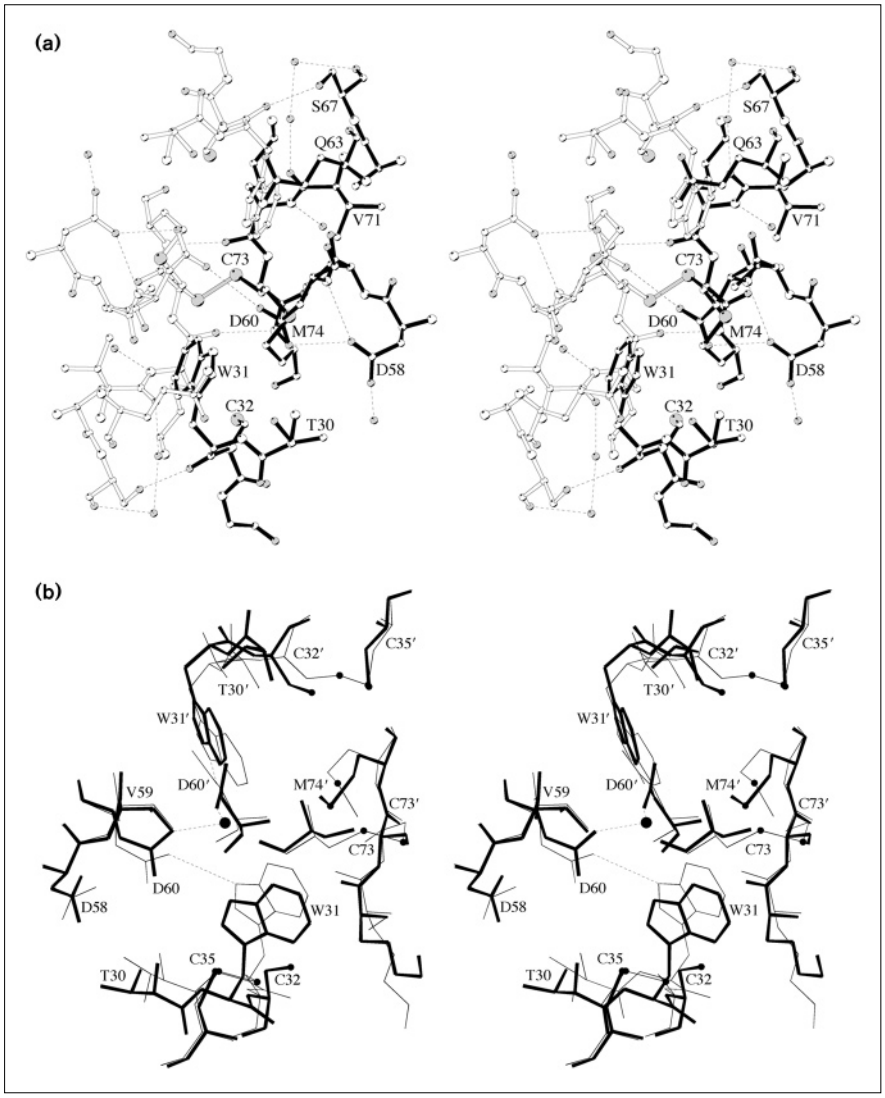

Stereoview of the thioredoxin dimer interface. (a) Trx-red viewed down the crystallographic twofold rotation axis. All twelve residues which make interchain contact are shown, as well as Asp58. (Labels for Val59, Ala66 and Lys72 are not included.) One monomer is shown in black, the other is outlined, and the Cys73–Cys73′ disulfide connection is in gray. Atom types are distinguished by circles of differing size (C = O < N < S), and shading (oxygen and sulfur are gray). Hydrogen bonds are indicated by dashed lines. (b) C73S (thick lines) superimposed with Trx-ox (thin lines), displaying the shifts in Trp31 and Asp60 that occur upon removal of the dimer interface disulfide bond or formation of a disulfide bond in the active site. Also shown is a water molecule that fills the gap between Trp31 and Trp31′ in C73S, represented as an isolated filled circle. (Figure produced with the program MOLSCRIPT [75].)

Reduced active site

Despite the wealth of data concerning thioredoxin, the mechanism by which the enzyme catalyzes disulfide exchange remains unclear [1]. Both the *E. coli* and human proteins display a depressed p*K*a for Cys32 (thought to be necessary for increasing the nucleophilicity of the thiolate group) and an elevated p*K*a for Cys35 [15,48,53]. Several possible mechanisms have been suggested for the reduced Cys32 p*K*a, including stabilization of the anionic form of Cys32 through hydrogen bonding between Cys32 and the amide of Cys35 [35], stabilization through interaction with the dipole of α helix 2 [19,54], and stabilization through hydrogen bonding to the Cys35 thiol [41]. Differences in the details of the human and *E. coli* thioredoxin NMR and X-ray structures have contributed to the uncertainty surrounding this question.

The present structures favor the model suggested by Dyson and co-workers [41] for the reduced pK_a of Cys32 in *E. coli* thioredoxin. In Trx-red, the Cys32 and Cys35 sulfhydryls are optimally aligned for hydrogen-bond formation, with Cys35 as the proton donor, and Cys32 as the acceptor (Fig. 7a). The distance between the two sulfhydryls is 3.9 Å, and the angles formed by Cys35Cβ–Cys35Sγ–Cys32Sγ and by Cys35Sγ–Cys32Sγ–Cys32Cβ are 105° and 70°, respectively. This arrangement is nearly identical to that for a similar hydrogen bond found in the crystal structure of L-cysteine, as determined by neutron diffraction [55]. In that structure, the corresponding distances and angles were 3.85 Å, 95.9°, and 69.8°, respectively. This hydrogen bond also occurs in the C73S structure, despite a change in the conformation of residues Ala29–Cys32 (discussed below). The pK_a of Cys32 is probably depressed as a consequence of this hydrogen bond.

Figure 6

Amino acid sequence alignment for vertebrate thioredoxins. Shown are the sequences for human [21,23], monkey [76], calf thymus [3], sheep [77], rabbit [44], mouse [21], rat [78], and chicken [79] thioredoxins. Methionine is shown in the first position, but is probably removed *in vivo* in vertebrate cells [3,44,45]. Invariant amino acids (63%) are shown in bold type, and the twelve amino acids of the dimer interface, ten of which are invariant (83%), are indicated with an asterisk.

```
          1                                    *  **                  50
  Human   MVKQIESKTA FQEALDAAGD KLVVVDFSAT WCGPCKMIKP FFHSLSEKYS
 Monkey   MVKQIESKAA FQEALDDAGD KLVVVDFSAT WCGPCKMIKP FFHSLSEKYS
   Calf   MVKQIESKYA FQEALNSAGE KLVVVDFSAT WCGPCKMIKP FFHSLSEKYS
  Sheep   MVKQIESKYA FQEALNSAGE KLVVVDFSAT WCGPCKMIKP FFHSLSEKYS
 Rabbit   MVKQIESKSA FQEVLDSAGD KLVVVDFSAT WCGPCKMIKP FFHALSEKFN
  Mouse   MVKLIESKEA FQEALAAAGD KLVVVDFSAT WCGPCKMIKP FFHSLCDKYS
    Rat   MVKLIESKEA FQEALAAAGD KLVVVDFSAT WCGPCKMIKP FFHSLCDKYS
Chicken   MVKSVGNLAD FEAELKAAGE KLVVVDFSAT WCGPCKMIKP FFHSLCDKFG

          51       **    *  **    ****                            105
  Human   NVIFLEVDVD DCQDVASECE VKCMPTFQFF KKGQKVGEFS GANKEKLEAT INELV
 Monkey   NVVFLEVDVD DCQDVASECE VKCMPTFQFF KKGQKVGEFS GANKEKLEAT INELV
   Calf   NVVFLEVDVD DCQDVAAEQE VKCMPTFQFF KKGQKVGEFS GANKEKLEAT INELI
  Sheep   NVVFLEVDVD DCQDVAAECE VKCMPTFQFF KKGQKVSEFS GANKEKLEAT INELI
 Rabbit   NVVFIEVDVD DCKDIAAECE VKCMPTFQFF KKGQKVGEFS GANKEKLEAT INELL
  Mouse   NVVFLEVDVD DCQDVAADCE VKCMPTFQFY KKGQKVGEFS GANKEKLEAS ITEYA
    Rat   NVVFLEVDVD DCQDVAADCE VKCMPTFQFY KKGQKVGEFS GANKEKLEAT ITEFA
Chicken   DVVFIEIDVD DAQDVATHCD VKCMPTFQFY KNGKKVQEFS GANKEKLEET IKSLV
```

The amide nitrogen of Cys35, which is hydrogen bonded to Cys32 in the NMR structure of hQM-Trx, is too far from the Cys32 sulfur for hydrogen bonding in either Trx-red or C73S (4.6 Å in both structures), although this hydrogen bond does occur in the oxidized protein (discussed below). The dipole of α helix 2 may also contribute to the reduced Cys32 pK_a. This dipole is pointed in the correct direction for stabilization of the Cys32 thiolate anion, but the Cys32 sulfhydryl is located on the edge of the helix (Fig. 7a) and therefore somewhat offset from the optimal alignment for stabilization. Thus, the major reason for the depressed Cys32 pK_a is probably the stabilization of the thiolate anion through hydrogen bonding to the Cys35 sulfhydryl, possibly with a small additional effect contributed by the dipole of α helix 2.

The basis for the increased pK_a of Cys35 is less controversial. Cys35 is almost completely buried in the present crystal structures, which disfavors deprotonation of the sulfhydryl. The depressed pK_a of Cys32 would also serve to elevate the pK_a of Cys35, as deprotonation of Cys32 would place a negative charge next to Cys35. The placement of Cys35 is due in part to a previously undetected hydrogen bond between the Cys35 sulfur and the amide nitrogen of Ala29 (3.7 Å in both Trx-red and C73S). These groups are perfectly aligned and at an acceptable distance

Figure 7

Stereoviews of (a) reduced and (b) oxidized human thioredoxin active sites. Atom types are distinguished by circles of differing size (C=O<N<S), and shading (oxygen and sulfur are in gray). Hydrogen bonds are indicated by dashed lines. (Figure produced with the program MOLSCRIPT [75].)

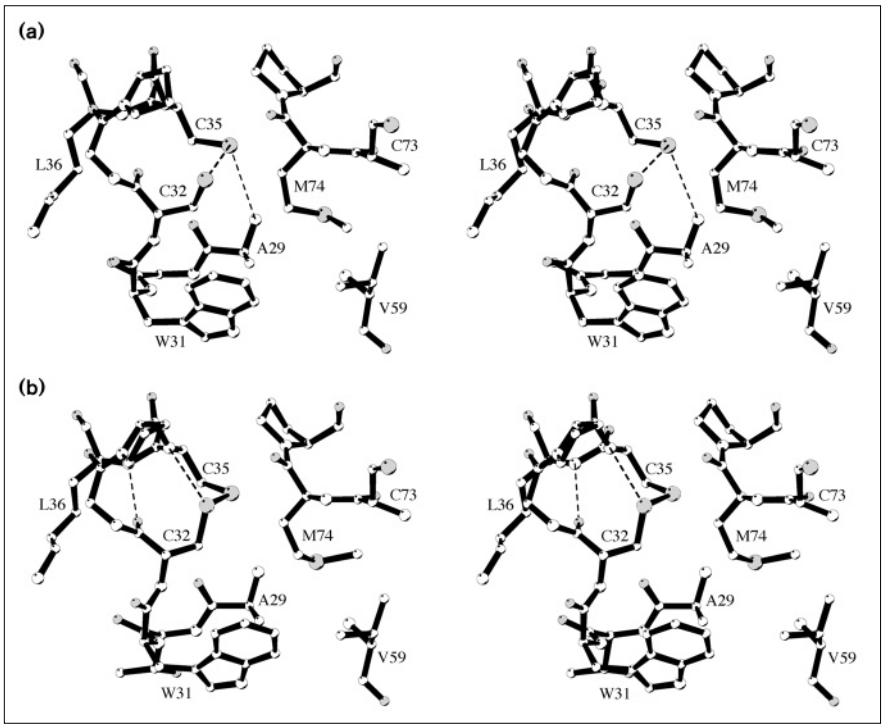

for hydrogen-bond formation [56]. The position of Cys35 is further restricted by its inclusion in α helix 2, and through numerous van der Waals contacts.

The conformation of the thioredoxin active site for the wild type human protein determined in the present study is very close to that found in the *E. coli* protein, especially with respect to the *E. coli* X-ray structure. In contrast, the active site in the hQM-Trx NMR structure is quite different than that of the present work. These differences may be due to the mutations in and near the thioredoxin active site. A detailed comparison of the known thioredoxin structures is presented in a later section.

C32S/C35S

As the placement of the active-site loop in the present structure was considerably different from that for the NMR structure, and as the placement of this loop is likely to be critical for thioredoxin function, we sought to further characterize it through the mutant protein C32S/C35S. This protein is inactive in catalysis and cell-growth stimulation, but is a competitive inhibitor of thioredoxin reductase, suggesting that the binding surface of the mutated protein is unimpaired [28]. Crystals of C32S/C35S were obtained under the same conditions as for the wild-type protein, and were isomorphous with those of the wild type. The difference electron density map calculated from the Trx-red and C32S/C35S diffraction data was largely flat except in the active site, where two large peaks corresponding to the sulfur atoms of Cys32 and Cys35 were found, as well as smaller peaks near neighboring residues (Fig. 1b).

Model building and refinement resulted in a structure for the mutant protein that was nearly identical to that of wild-type protein, except in the active site. Shifts in active-site residues Ala29–Ser35 in the mutant move the hydroxyl of Ser32 into van der Waals contact with the hydroxyl of Ser35 (3.4 Å), and possibly also lead to hydrogen-bond formation between the Ser32 hydroxyl and the amide nitrogen of Ser35 (3.3 Å). The side chain of Trp31 occupies a new position about 1.3 Å away from its position in Trx-red. Small shifts in nearby residues accompany those of Ala29–Ser35 allowing appropriate van der Waals contacts to be maintained. For example, Met74 appears to track the position of Trp31 by changing the conformation of its side chain.

The observed active-site conformation for C32S/C35S is very similar to that of Trx-ox (discussed below), suggesting that the conformational change observed upon oxidation occurs simply by allowing Cys32 and Cys35 to move closer together. For example, the hydrogen bond formed between the Ser35 amide and the Ser32 hydroxyl is very similar to that formed by the amide and the sulfur of Cys32 in Trx-ox. Most interesting in this regard is the position and degree of order observed for Trp31, which is partially disordered in Trx-red and C73S, but fairly well ordered in C32S/C35S and Trx-ox. This suggests that Ala29–Cys32 settle into a single conformation simply by removing the steric conflict between the sulfhydryls of Cys32 and Cys35, rather than through formation of a disulfide bond across this span of amino acids. It is possible that the resemblance of C32S/C35S to the oxidized wild-type protein contributes to its ability to act as a competitive inhibitor of thioredoxin reductase [28].

There is also a change in the hydrogen bonding of the dimer interface in C32S/C35S. The hydrogen bond between Glu58 and Asp60 (Fig. 5a) has been replaced by hydrogen bonds from each residue to an ordered water molecule which, in turn, forms two additional hydrogen bonds to the amide nitrogen and side-chain hydroxyl of Thr30 (not shown). The four hydrogen bonds formed by this water molecule range from 2.7 to 3.0 Å in length. In the oxidized structure, Asp60 hydrogen bonds to Trp31 (see below).

Oxidized thioredoxin

We pursued the structure of oxidized thioredoxin in order to assess changes in the active site upon disulfide-bond formation. The approach taken, as reductant was required for crystal formation, was to allow spontaneous oxidation to occur in crystals of reduced thioredoxin by storing the crystals in solution without replenishing the reductant DTT. Such crystals diffracted beyond 2.0 Å resolution despite a doubling of the mosaic spread (to 1.0°), and a slight change in cell constants (Table 1). A comparison of amplitudes from an oxidized crystal and Trx-red yielded a merging R factor of 0.20, higher than the values obtained with the two mutated protein crystals (Table 1).

The difference electron density map between Trx-red and the oxidized crystal revealed numerous peaks (Fig. 1c,d), the most prominent of which was between the Cys32 and Cys35 sulfhydryls of the Trx-red model (Fig. 1d), indicating that Cys32 and Cys35 were disulfide linked in Trx-ox. Smaller difference peaks in the active site indicated a conformational change similar to that which occurred in C32S/C35S. A model for the oxidized protein was thus built and refined with this disulfide bond in place. The final electron-density map for this model was of somewhat lower quality than that of the other structures. Likewise, R-free for the structure, which provides an unbiased comparison of the observed and modeled structure factor amplitudes, was higher than expected for a well refined structure. Therefore the Trx-ox model must be regarded as less reliable than the other thioredoxin models. That there are no major errors in the placement of atoms in the final Trx-ox model was confirmed through inspection of the Trx-red–Trx-ox difference electron density map (Fig. 1), and the phase-bias-removed 'omit' electron density maps (see the Materials and methods

section). It is unclear why R-free is high for these data, but this may be related to the high mosaic spread of the oxidized crystals, or possibly to an anisotropic disorder in the crystal, as was recently described by Sheldrick and coworkers for cytochrome c_6 [57].

Numerous small differences occurred in the active site and dimer interface of Trx-ox with respect to Trx-red, but in general the structures were very similar (the rms deviation in Cα positions was only 0.26 Å). To form the disulfide bond, Cys32 moved toward Cys35 through shifts in Ala29–Cys35, much like that which occurred in the C32S/C35S mutant structure. Cys35 moved slightly toward Cys32 on forming the disulfide bond, which had a bond length of 2.0 Å in the final model. The largest movement was in the indole ring of Trp31, which shifted about 1 Å away from its position in Trx-red, and was accompanied by a reorientation in the side-chain conformation of Met74. The electron density for the main-chain atoms of Trp31 was better defined in Trx-ox than in either Trx-red or C73S, and of similar quality to that of C32S/C35S, where a similar conformation for the residue is found. However, the electron density for Cβ of Cys35 was of lesser quality in Trx-ox than in the other structures where it was excellent (see Fig. 1a). The positions for these groups are stabilized by a hydrogen bond between the sulfur of Cys32 and the amide nitrogen of Cys35 (3.2 Å, Fig. 7b). As mentioned above, this hydrogen bond is absent in the reduced structure where the two groups lie well apart (4.6 Å). This hydrogen bond also occurs in the oxidized *E. coli* thioredoxin X-ray and NMR models, as well as in the models of the oxidized and reduced hQM-Trx, but not in the reduced *E. coli* NMR model.

An interesting change also occurs in the dimer interface of Trx-ox as compared with Trx-red. The Asp60–Asp60′ hydrogen bond of Trx-red (Fig. 5a) has been replaced by a hydrogen bond between Asp60 and the indole nitrogen of Trp31 in each monomer of Trx-ox (Fig. 5b). A similar hydrogen bond occurs in the crystal structure of oxidized *E. coli* thioredoxin. In contrast to our observation, the NMR groups not only report this hydrogen bond to be present in the oxidized human and *E. coli* proteins [34,35], but also in the reduced proteins, although it should be noted that the geometry for such hydrogen bonding is poor in both the human model and in the low resolution *E. coli* model [58], which is the only *E. coli* NMR model available at present in the protein data bank.

Comparison of reduced, oxidized and mutant structures

The four thioredoxin structures determined in the present work have the same general structure, and all are dimers. The rms deviation between Cα positions ranges from 0.13 Å (between C73S and Trx-red) to 0.33 Å (between C73S and Trx-ox). The main differences among them occur in active-site residues Ala29–Cys35, and in dimer interface residues Lys72–Met74. The most pronounced movement occurs at Trp31, which lies both in the active site and in the dimer interface. Upon oxidation, Trp31 moves across the active site towards Met74 (Fig. 8a), and across the dimer interface toward Trp31′ of the second monomer (Fig. 5b). The distance between Trp31 and Trp31′ (measured between side-chain atoms CZ2 from each monomer) is 6.2, 5.6, 4.0 and 3.8 Å for the structures C73S, Trx-red, Trx-ox, and C32S/C35S, respectively. Thus, as Cys32 and Cys35 move closer together, so too do Trp31 and Trp31′, eventually contacting one another in the dimer interface.

To accomplish this conformational change, residues Ala29–Cys35 pivot about the sulfur of Cys35, which does not change in position, resulting in a more closed active site (Fig. 8a). The double mutant C32S/C35S undergoes a similar conformational change to that of Trx-ox, suggesting that the pivot motion about Cys35 in the wild-type protein simply requires the occurrence of a reduction in the distance between the two active-site sulfhydryls. Contacts among residues in the dimer interface apparently induce a partial closure of the active site, as removal of the disulfide bond between Cys73 and Cys73′ in C73S causes a slight relaxation in the dimer interface, allowing active-site residues Ala29–Cys35 to pivot to a more open position than found in Trx-red (Figs 5b,8a). Despite this shift, the hydrogen bond between the active-site sulfhydryls remains in place in the C73S structure (3.8 Å).

Two additional consequences of oxidation and conformational change in the thioredoxin active site are the tightening of α helix 2, and the loss of a hydrogen bond to the Cys35 sulfhydryl. The carbonyls of Cys32 and Gly33 form well-aligned hydrogen bonds to the amide nitrogens of Lys36 and Met37, respectively, in the first turn of α helix 2 in the oxidized structure (3.2 and 2.9 Å, respectively), but the first of these is lost (3.5 Å) and the second weakened (3.2 Å) in the reduced structure. The shift in the Cys32 and Gly33 carbonyls can be seen in Figure 8a. In contrast, the hydrogen bond between the sulfhydryl of Cys35 and the amide of Ala29 (3.7 Å apart in Trx-red) is lost upon oxidation (4.2 Å apart in Trx-ox). This balancing of hydrogen bonds may help to ensure the reversibility of thioredoxin oxidation and reduction.

Comparison with other thioredoxin structures

All known structures of thioredoxin, whether determined by NMR or X-ray diffraction techniques, have the same general fold. Differences among the structures do exist, however, especially in the exterior loops of the protein, including that of the active site (Fig. 8b). The thioredoxin fold consists of a core five-stranded β sheet flanked by four α helices (Fig. 3). The active-site peptide Ala29–Lys36 includes the end of β strand 2, two to three linking amino acids, and the beginning of α helix 2. The rms deviation in

Figure 8

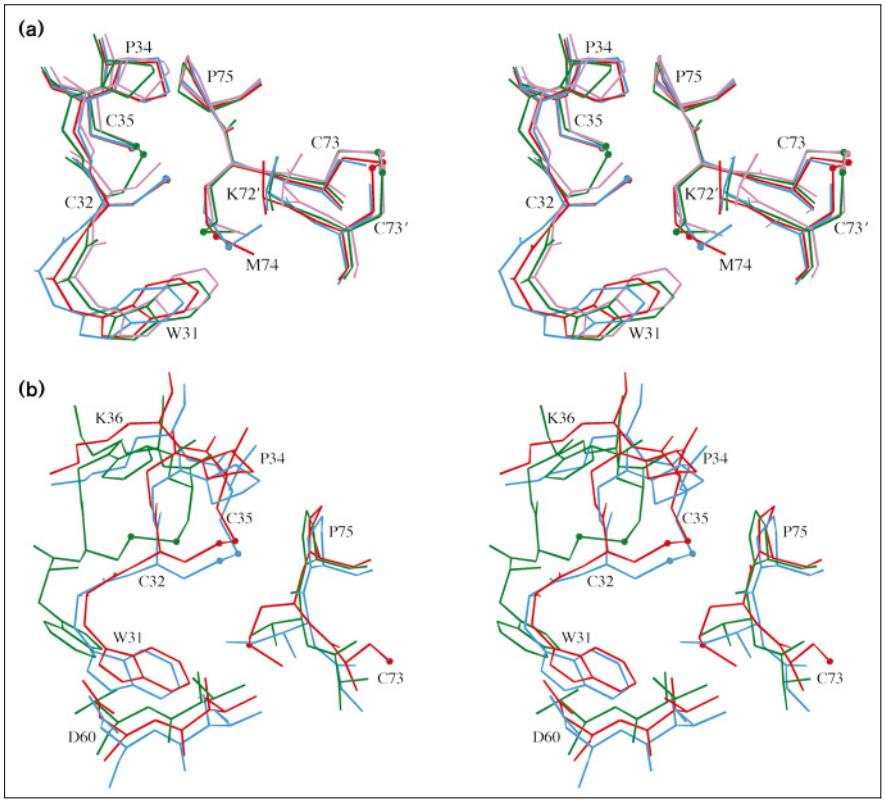

Stereoviews of the differences among the thioredoxin active sites, after superposition. (a) Residues Trp31–Cys35, Cys73–Pro75, and Lys72′–Cys73′ (from the other monomer) for C73S (blue), Trx-red (red), Trx-ox (green), and C32S/C35S (pink). (b) Trp31–Lys36, Val59–Asp60 and Cys73–Pro75 for the hQM-Trx (NMR, green), human Trx-ox (X-ray, red) and *E. coli* (X-ray, blue). Cαs from residues 1–27 and 38–105 were used to superimpose the oxidized hQM-Trx structure with Trx-ox, and the Cαs of the β sheet were used to superimpose the *E. coli* crystal structure with Trx-ox. (Figure produced with the program MOLSCRIPT [75].)

Cα positions between Trx-red and the average NMR structure for reduced hQM-Trx is 1.2 Å, and the two structures are sufficiently similar to have allowed a structure determination by molecular replacement (using the nearly identical single mutant NMR structure).

Despite these similarities, the distribution of differences between the two structures was decidedly non-random (Fig. 9a). The largest differences occur in the active-site peptide Ala29–Lys36, where deviations greater than 3 Å occur. The smallest deviations are in the β sheet, which displayed an rms deviation of 0.51 Å. Both the position and conformation of the Cys32/Cys35-containing active-site loop differs in Trx-red with respect to the same loop in the hQM-Trx NMR structure. Conformational differences occur in residues Ala29 and Thr30, where ψ differs by ~30°; in Ser28, where an additional hydrogen bond at the end of β strand 2 occurs in the X-ray structure (2.9 Å); and in α helix 2 (residues 33–47), where there is a noticeable regularization in hydrogen bonding in Trx-red. The altered conformation in these residues is coupled with additional shifts in the amino acids they contact, including residues 74–75, and 92–97.

We also compared the human and *E. coli* thioredoxin structures. To do so, we superimposed residues 23–48, and 52–93 (numbering corresponds to that of the human sequence), as these residues were the least affected by insertions and deletions. Unexpectedly, both the *E. coli* reduced NMR structure (1.11 Å rms deviation) and the *E. coli* oxidized X-ray structure (0.79 Å and 0.81 Å rms deviation for monomer 1 and 2, respectively) were in better agreement with Trx-red for these 68 residues than the human NMR structure (1.19 Å rms deviation). This trend was even more pronounced for the cysteine-containing peptide that spans the active site: rms deviations were 1.08, 0.80, and 0.34 Å for the Cα positions of residues 28–38 for the human NMR, the *E. coli* NMR, and the *E. coli* X-ray structures, respectively, when fitted to the same residues in Trx-red. Similar deviations resulted upon comparison of the equivalent oxidized structures. Thus, despite having only 27% sequence identity, the two X-ray structures are in better agreement than any other pair of structures. Possibly this is a reflection of the high resolution for the two X-ray structures (~1.7 Å in both cases). It should be noted that the low-resolution *E. coli* thioredoxin NMR structure [58] was used in the comparison, as the high-resolution structure [34] is not yet available. Figure 8b shows the thioredoxin active site for three of the oxidized structures after superposition of the β sheet regions of the proteins.

Several factors should be noted when comparing the X-ray and NMR structures of the human thioredoxin active site. In the X-ray structure the active site is blocked by dimer

Figure 9

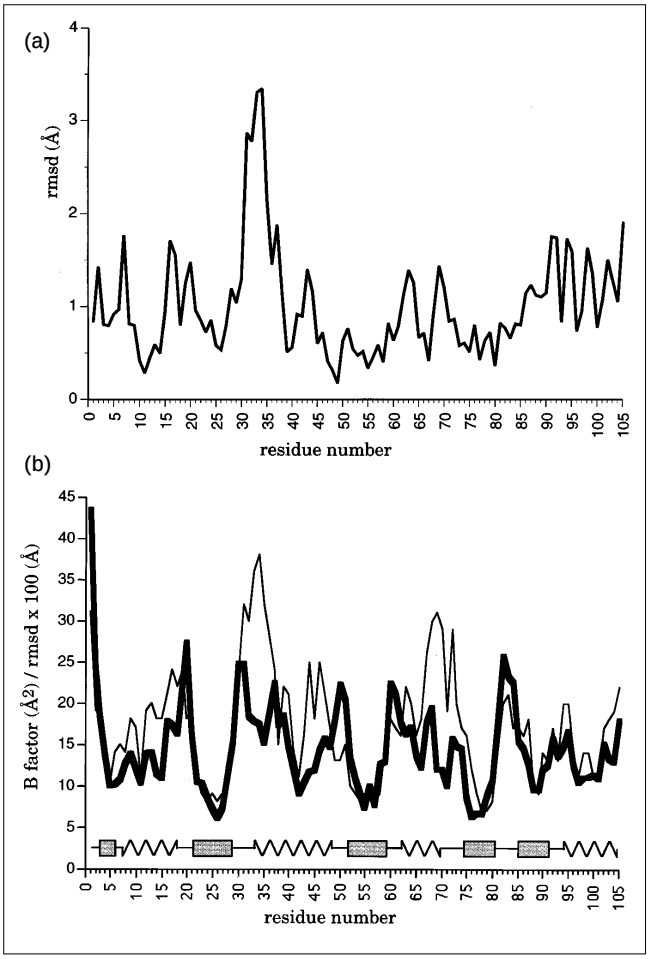

Comparisons of the solution and crystal structures of reduced thioredoxin. (a) Rms deviation between Cα atoms for Trx-red and the reduced hQM-Trx NMR structure, after superposition. All Cα atoms were used for superposition. (b) Plot of Cα temperature factors for Trx-red (Å^2, thick line), and Cα rms deviations among the 40 NMR structures generated for the hQM-Trx (Å×100, thin line). Regions of secondary structure in the thioredoxin monomer are indicated by stippled boxes (β-sheet strands) and zigzags (α helices).

formation, and Trp31 is completely buried in the dimer interface. Such contacts could alter the conformation of the Cys32–Cys35-containing loop. As discussed above and shown in Figure 8a, this region of the protein displays conformational flexibility despite contacts in the dimer interface. However, a comparison of the C73S and Trx-red structures suggests additional conformations may exist. That the active-site conformation we see for dimeric human thioredoxin is likely to occur for the monomeric protein is supported by its remarkable similarity to the active site of the monomeric *E. coli* thioredoxin X-ray structure. These structures retain nearly identical active sites despite low sequence identity, dissimilar crystal forms, and dissimilar intermolecular contacts near the active site in the crystal.

The protein used in the NMR study contains four altered amino acids with respect to the wild-type protein (C62A, C69A, C73A, M74T), is active, and has recently been shown to form a mixed disulfide with a peptide from the thioredoxin redox partner NFκB [36]. The conformation seen in the crystal structure of the wild-type protein is not among the 40 structure ensemble produced in the NMR study (PDB entry 1trv). The reason for the differences in the structures is not clear but may in part be due to the M74T mutation, as Met74 makes numerous contacts with Trp31 in the X-ray structure, and the M74T single mutant NMR structure is very similar to that of the quadruple mutant [34]. In the reduced X-ray structure, Val59, Ala29, Trp31, and Cys32 all pack around the side chain of Met74, while in the more open active site of the NMR structure, only Val59 contacts Thr74 (Fig. 8b). It should also be noted that the sulfurs of Cys32 and Cys35 are unusually close together in the NMR structures (3.1 Å), and that all of the mutation sites (Cys62, Cys69, Cys73, and Met74) and some residues in contact with the mutation sites (e.g. Ser7) display local conformational shifts (Fig. 9a).

We compared the rms deviations in the NMR structure ensemble, which are related to conformational mobility in solution, to the crystallographic temperature (B) factors, which are related to conformational mobility in the crystal. As shown in Figure 9b, the correspondence of the two plots is fairly high. For example, the β sheet is the best ordered portion in both structures. Two portions of the plots that show greater than average deviations in the NMR structure, but display temperature factors close to the mean in the X-ray structure, are residues 29–39 and 66–75, both of which pass through the thioredoxin active site and are in structurally different conformations in the two structures. A possible explanation for this is that the M74T mutation in the protein used in the NMR study led to greater mobility in these residues through loss of contacts to the methionine side chain, as described above.

Concluding remarks

We have determined four crystal structures of human thioredoxin, all of which were dimeric in the crystal and, except for the C73S mutant, covalently linked through a disulfide bond. Several factors suggest the thioredoxin homodimer may play a physiological, possibly regulatory, role. First, the residues that occupy the dimer interface are more highly conserved than the rest of the protein among vertebrate thioredoxins. Second, covalently linked dimers are readily formed at thioredoxin concentrations above 125 mM, even in the presence of the reducing agent DTT. Third, wild-type thioredoxin rapidly loses its biological activity (ability to stimulate cell growth) upon storage in the absence of reducing agent (JR Gasdaska *et al.*, unpublished data), whereas the mutant C73S retains its biological activity upon storage. Fourth, the dimeric form of thioredoxin is not a substrate for thioredoxin

reductase. Fifth, Cys73 is required for thioredoxin to function as a part of the early pregnancy factor [50], one of several newly discovered extracellular functions for the protein. Experiments are under way to determine what role, if any, dimer formation plays.

Insight into extracellular function might also be gained through comparison of thioredoxins from different species. Human and *E. coli* thioredoxins display remarkably similar structures, but do not function identically, especially with respect to autocrine activity. Human thioredoxin can stimulate a variety of tumor-derived cell lines to grow in the absence of added serum, whereas *E. coli* thioredoxin, at least for the breast cancer cell line MCF-7 [11], cannot. *E. coli* thioredoxin can produce a transient increase in DNA synthesis by human lymphoid cells in the presence of serum [59], and so is not completely without extracellular activity. Both redox activity and reduction by an extracellular thioredoxin reductase is apparently required for thioredoxin growth stimulation [28]; however both proteins can serve as substrates for human thioredoxin reductase [60], and therefore their reduced forms can presumably be regenerated at the cell surface. The dimeric form of human thioredoxin is apparently not required for growth stimulation as dimer formation blocks the active site, and the C73S mutant protein, which is less prone to dimerization, is fully active (Gasdaska *et al.*, unpublished data). The surface amino acids of *E. coli* and human thioredoxins are quite different away from the active site and these differences are likely to be responsible for the lack of autocrine activity in the *E. coli* protein. It is possible that the *E. coli* protein does not bind to one or more of the cell surface proteins necessary for initiating the growth signal, and thus cannot reduce a key signaling intermediate.

Biological implications

Thioredoxin is a ubiquitous oxidoreductase implicated in an increasingly large number of biological activities, including regulation of transcription factors such as NFκB, and autocrine growth stimulation in some tumors. The four crystal structures of human thioredoxin reported here provide new insight into the thioredoxin mechanism and reveal a previously unknown dimeric form of the protein.

The physiological role, if any, of thioredoxin-dimer formation remains unclear. Small amounts of thioredoxin dimer have been detected in cells ([37]; G Powis, unpublished observations). It is possible that oxidant-induced dimer formation is a method of sensing oxidizing conditions in the cell: dimer formation removes thioredoxin from the redox cycle catalyzed by thioredoxin reductase, as the dimer is not a substrate for this enzyme [37]. Dimerization of secreted thioredoxin in the relatively oxidizing extracellular environment could be a way of limiting the growth stimulating effects of thioredoxin: the thioredoxin dimer does not stimulate cell proliferation (JR Gasdaska *et al.*, unpublished data).

The evidence reviewed previously that thioredoxin is important for cell proliferation and cell transformation, and the finding that some human cancers show greatly increased thioredoxin gene expression [22,23], suggest that thioredoxin could be a target for anti-cancer drug development. X-ray crystallographic studies are under way to aid in the design of such inhibitors.

Materials and methods

Crystallization and diffraction measurement

Wild-type and mutant human thioredoxins were expressed and purified as previously described ([11,28], Gasdaska *et al.*, unpublished data). Amicon 3k MCO filters were used to concentrate and equilibrate the proteins with 10 mM sodium acetate buffer (pH 3.8) supplemented with 5 mM DTT. Rhombohedral crystals were grown by the hanging drop method from a solution containing 10 mM sodium acetate buffer (pH 3.8), 25% (v/v) 2-methyl-2,4-pentanediol (MPD), 5 mM DTT, and equilibrated at room temperature against the same solution with 50% MPD. The initial protein concentrations in the crystallization drops were 5, 4, and 6 mg ml^{-1} for wild-type, C32S/C35S, and C73S proteins, respectively. Crystals of Trx-red measuring approximately $0.4\times0.2\times0.2$ mm were obtained after three days by seeding small (<0.05 mm) crystals into drops pre-equilibrated for approximately 2 h against the precipitant solution. Such crystals diffracted beyond 1.7 Å resolution, were stable in the X-ray beam for several days, and were stable in the crystallization drop at room temperature for several months. Crystals of Trx-ox were obtained by allowing crystals with reduced active-site sulfhydryls to oxidize in the crystallization drop for approximately two months by withholding the addition of fresh DTT. The oxidized crystals displayed a twofold increase in mosaic spread, but still diffracted beyond 2.0 Å resolution.

X-ray diffraction data were measured at room temperature using a FAST area detector with graphite monochromated CuKα radiation generated from an Enraf-Nonius FR571 rotating anode. Each diffraction image was recorded for 60–100 s while rotating the crystal through 0.15° in omega. Intensities were estimated using the programs MADNES [61], PROCOR [62], and FBSCALE [63]. The crystal and data collection results are summarized in Table 1.

Although human thioredoxin was crystallized under conditions similar to those for the *E. coli* protein [64] the crystals were not isomorphous with those of *E. coli* thioredoxin. The presence of 1 mM Cu^{2+}, an important component in the *E. coli* thioredoxin crystallization, did not affect formation of the human thioredoxin crystals.

Structure determinations

The crystal structure of Trx-red was determined through molecular replacement using the NMR human M74T mutant thioredoxin structure as a starting model (using the average NMR structure, PDB entry 3TRX [43]). Rotation and translation searches were carried out with X-PLOR [65]. The rotation search, performed with data between 15 and 2.8 Å and filtered with 20 steps of Patterson correlation refinement, resulted in a single peak well above all other peaks that eventually proved to be the correct solution. The translation search was restricted to the x/z plane of the unit cell, which is all that is required in space group C2. The best solution had a crystallographic residual (R-factor) of 0.52, a correlation coefficient value of 0.31, and was statistically much better than the next closest peak, which had a correlation coefficient of 0.20. Rigid-body refinement reduced the R-factor slightly to 0.50. Simulated annealing using a slow-cooling protocol for 3σ data between 15 and 2.8 Å was more successful and reduced the R-factor to 0.27.

Parameter files distributed with X-PLOR version 3.1 were used (param19x.pro and toph19x.pro). A $2F_o–F_c$ electron-density map calculated at this stage revealed clear electron density for most of the structure, but no density for the fragment between amino acids 30 and 36. Cycles of refinement alternated with manual correction of the protein model and the incremental inclusion of higher resolution data resulted in improved electron density for the model, and revealed a new position for residues 30–36. An intermolecular disulfide bond was also discovered involving Cys73 and Cys73′ of the crystallographically twofold-related monomer, as well as good density for Met74, which had been left in the mutant form of the protein (threonine) to this stage. During rebuilding, the side chains of Asp20, His43, and Ser90 were found to occupy two conformations, and have been built and refined as such. Statistics concerning the final 1.7 Å model can be found in Table 1.

Crystals of the mutant thioredoxins C73S and C32S/C35S were isomorphous with those of the wild-type protein, which allowed the Trx-red model to be used as a starting model in the refinement of both structures. New positions were found for residues in the active site and dimer interface, and modeled as such. Two conformations for Ser90 were included in the final refinement of the C73S mutant, and for His43 in C32S/C35S.

A crystal of wild-type thioredoxin allowed to oxidize for two months was used to collect diffraction data to a resolution of 2.1 Å (reductant was required for crystallization). The oxidized crystals did not diffract as well as the reduced crystals and had a doubling in the mosaic spread (to 1.0°), but displayed acceptable agreement among symmetry related reflections (R_{sym}=0.049). A difference electron density map between Trx-red and these data revealed a strong positive peak between the sulfur atoms of cysteines 32 and 35, confirming the presence of a disulfide bond between the two residues, and numerous smaller peaks consistent with a conformational change in the active site similar to that found for C32S/C35S. The structure was refined using X-PLOR with a constrained distance for the active site disulfide bond. The $2F_o–F_c$ electron-density maps were fully interpretable for manual adjustment of the model, but were of somewhat lower quality than those for the other three structures. Unbiased omit maps, where atoms under consideration were omitted from the model and phase bias removed by either simulated annealing with X-PLOR or refinement with GPRLSA [66,67], were used in the positioning of all atoms. The final $F_o–F_c$ electron-density map was essentially flat above the noise level, and no residual positive or negative peaks occurred at any of the sulfur positions. The final model displayed excellent stereochemistry, good agreement with the difference Fourier between Trx-red and Trx-ox, and an acceptable R-cryst (0.22). However R-free was higher than expected for a well refined model (0.33). The reason for the high R-free is unclear but is possibly related to an unmodeled disorder in the crystal, which may also have given rise to the high mosaic spread observed for these crystals. Although the difference between R-free and R-cryst suggests overfitting of the model, all parameters released during refinement resulted in a reduction of both R-free and R-cryst. Only 36 water molecules were included in the final model, and the temperature factors for connected atoms were highly correlated (correlation coefficient=0.94). A similar structure determination under way in our laboratory with an inhibited form of the oxidized protein displays similar refinement statistics, suggesting that the problem is a general component of the oxidized crystals (data not shown). That no major errors occur in the Trx-ox model was confirmed through the use of unbiased omit maps, as described above. However, because of the high R-free, the Trx-ox model must be considered less accurate than the other three Trx structures.

The Cys73–Cys73′ dimer interface disulfide bond lengths were not constrained during refinement, resulting in slightly incorrect distances between the bonded sulfurs (~2.3 Å in all three models). The Cys73 sulfur positions were manually shifted to yield more appropriate bond lengths in the final models (2.0 Å). The new sulfur positions were in good agreement with the electron density for these atoms (Fig. 2).

The positions for all amino acids were checked using ‘omit’ maps. Model geometry was checked with PROCHECK [68] and all four models had at least 92% of their amino acids in the most favorable regions of a Ramachandran plot. Statistics concerning the geometry of the final models are given in Table 1. Structures were superimposed and rms deviations calculated using the programs INSIGHTII [69] and X-PLOR [65]. The fractional accessibility of protein atoms to solvent and the surface area of the dimer interface were calculated with the program GRASP [70]. Model building was performed with FRODO [71,72] and general crystallographic calculations performed with CCP4 [73]. Sequence alignments were obtained with GCG [74].

Accession numbers

Coordinates have been deposited with the Protein Data Bank, and have accession numbers 1ert (reduced thioredoxin); 1eru (oxidized thioredoxin); 1erv (C73S mutant thioredoxin) and 1erw (C32S/C35S mutant thioredoxin).

Acknowledgements

This work was supported in part by American Cancer Society grant DHP-45 (WRM) and NIH grant CA 48725 (GP).

References

1. Holmgren, A. (1995). Thioredoxin structure and mechanism: conformational changes on oxidation of the active-site sulfhydryls to a disulfide. *Structure* **3**, 239–243.
2. Holmgren, A. (1989). Thioredoxin and glutaredoxin systems. *J. Biol. Chem.* **264**, 13963–13966.
3. Eklund, H., Gleason, F.K. & Holmgren, A. (1991). Structural and functional relations among thioredoxins of different species. *Proteins* **11**, 13–28.
4. Martin, J.L. (1995). Thioredoxin – a fold for all reasons. *Structure* **3**, 245–250.
5. Matthews, J.R., Wakasugi, N., Virelizier, J.-L., Yodoi, J. & Hay, R.T. (1992). Thioredoxin regulates the DNA binding activity of NF-κB by reduction of a disulphide bond involving cysteine 62. *Nucleic Acids Res.* **20**, 3821–3830.
6. Grippo, J.F., Tienrungroj, W., Dahmer, M.K., Housley, P. & Pratt, W.B. (1983). Evidence that the endogenous heat-stable glucocorticoid receptor-activating factor is thioredoxin. *J. Biol. Chem.* **258**, 13658–13664.
7. Xanthoudakis, S., Miao, G., Wang, F., Pan, Y.-C.E. & Curran, T. (1992). Redox activation of Fos–Jun DNA binding activity is mediated by a DNA repair enzyme. *EMBO J.* **11**, 3323–3335.
8. Edman, J.C., Ellis, L., Blacher, R.W., Roth, R.A. & Rutter, W.J. (1985). Sequence of protein disulphide isomerase and implications of its relationship to thioredoxin. *Nature* **317**, 267–270.
9. Martin, J.L., Bardwell, J.C. & Kuriyan, J. (1993). Crystal structure of the DsbA protein required for disulphide bond formation *in vivo*. *Nature* **365**, 464–468.
10. Boniface, J.J. & Reichert, L.E.J. (1990). Evidence for a novel thioredoxin-like catalytic property of gonadotropic hormones. *Science* **247**, 61–64.
11. Gasdaska, J.R., Berggren, M. & Powis, G. (1995). Cell growth stimulation by the redox protein thioredoxin occurs by a novel helper mechanism. *Cell Growth Differ.* **6**, 1643–1650.
12. Deiss, L.P. & Kimchi, A. (1991). A genetic tool used to identify thioredoxin as a mediator of a growth inhibitory signal. *Science* **252**, 117–120.
13. Clarke, F.M., *et al*., & Wells, J.R. (1991). Identification of molecules involved in the ‘early pregnancy factor’ phenomenon. *J. Reprod. Fert.* **93**, 525–539.
14. Yoshitake, S., Nanri, H., Fernando, M.R. & Minakami, S. (1994). Possible differences in the regenerative roles played by thioltransferase and thioredoxin for oxidatively damaged proteins. *J. Biochem.* **116**, 42–46.
15. Forman-Kay, J.D., Clore, G.M. & Gronenborn, A.M. (1992). Relationship between electrostatics and redox function in human thioredoxin: characterization of pH titration shifts using two-dimensional homo- and heteronuclear NMR. *Biochemistry* **31**, 3442–3452.
16. Nelson, J.W. & Creighton, T.E. (1994). Reactivity and ionization of the active site cysteine residues of DsbA, a protein required for disulfide bond formation *in vivo*. *Biochemistry* **33**, 5974–5983.

17. Lundstrom, J., Krause, G. & Holmgren, A. (1992). A Pro to His mutation in active site of thioredoxin increases its disulfide-isomerase activity 10-fold. *J. Biol. Chem.* 267, 9047–9052.
18. Grauschopf, U., Winther, J.R., Korber, P., Zander, T., Dallinger, P. & Bardwell, J.C.A. (1995). Why is DsbA such an oxidizing disulfide catalyst? *Cell* 83, 947–955.
19. Kortemme, T. & Creighton, T.E. (1995). Ionisation of cysteine residues at the termini of model α-helical peptides. Relevance to unusual thiol pK_a values in proteins of the thioredoxin family. *J. Mol. Biol.* 253, 799–812.
20. Gane, P.J., Freedman, R.B. & Warwicker, J. (1995). A molecular model for the redox potential difference between thioredoxin and DsbA, based on electrostatics calculations. *J. Mol. Biol.* 249, 376–387.
21. Tagaya, Y., *et al.*, & Yodoi, J. (1989). ATL-derived factor (ADF), an IL-2 receptor/Tac inducer homologous to thioredoxin; possible involvement of dithiol-reduction in the IL-2 receptor induction. *EMBO J.* 8, 757–764.
22. Fujii, S., *et al.*, & Yodoi, J. (1991). Coexpression of adult T-cell leukemia-derived factor, a human thioredoxin homologue, and human papillomavirus DNA in neoplastic cervical squamous epithelium. *Cancer* 68, 1583–1591.
23. Gasdaska, P.Y., Oblong, J.E., Cotgreave, I.A. & Powis, G. (1994). The predicted amino acid sequence of human thioredoxin is identical to that of the autocrine growth factor human adult T-cell derived factor (ADF): thioredoxin mRNA is elevated in some human tumors. *Biochim. Biophys. Acta* 1218, 292–296.
24. Nakamura, H., *et al.*, & Yodoi, J. (1992). Expression and growth promoting effect of adult T-cell leukemia-derived factor: a human thioredoxin homologue in hepatocellular carcinoma. *Cancer* 69, 2091–2097.
25. Ericson, M.L., Horling, J., Wendel-Hansen, V., Holmgren, A. & Rosen, A. (1992). Secretion of thioredoxin after *in vivo* activation of human B cells. *Lymphokine Cytokine Res.* 11, 201–207.
26. Rubartelli, A., Bajetto, A., Allavena, G., Wollman, E. & Sitia, R. (1992). Secretion of thioredoxin by normal and neoplastic cells through a leaderless secretory pathway. *J. Biol. Chem.* 267, 24161–24164.
27. Rubartelli, A., Bonifaci, N. & Sitia, R. (1995). High rates of thioredoxin secretion correlate with growth arrest in hepatoma cells. *Cancer Res.* 55, 675–680.
28. Oblong, J.E., Berggren, M., Gasdaska, P.Y. & Powis, G. (1994). Site-directed mutagenesis of active site cysteines in human thioredoxin produces competitive inhibitors of human thioredoxin reductase and elimination of mitogenic properties of thioredoxin. *J. Biol. Chem.* 269, 11714–11720.
29. Kirkpatrick, D.L., Jimale, M.L., King, K.M. & Chen, T. (1992). Synthesis and evaluation of imidazolyl disulfides for selective cytotoxicity to hypoxic EMT6 tumor cells *in vitro*. *Eur. J. Med. Chem.* 27, 33–37.
30. Oblong, J., *et al.*, & Powis, G. (1994). Reversible inhibition of human thioredoxin reductase activity by cytotoxic alkyl 2-imidazolyl disulfide analogues. *Cancer Chemother. Pharmacol.* 34, 434–438.
31. Katti, S.K., LeMaster, D.M. & Eklund, H. (1990). Crystal structure of thioredoxin from *Escherichia coli* at 1.68 Å resolution. *J. Mol. Biol.* 212, 167–184.
32. Holmgren, A., Söderberg, B.-O., Eklund, H. & Brändén, C.-I. (1975). Three-dimensional structure of *Escherichia coli* thioredoxin-S2 to 2.8 Å resolution. *Proc. Natl. Acad. Sci. USA* 72, 2305–2309.
33. Saarinen, M., Gleason, F.K. & Eklund, H. (1995). Crystal structure of thioredoxin-2 from *Anabaena*. *Structure* 3, 1097–1108.
34. Jeng, M.F., *et al.*, & Dyson, H.J. (1994). High-resolution solution structures of oxidized and reduced *Escherichia coli* thioredoxin. *Structure* 2, 853–868.
35. Qin, J., Clore, G.M. & Gronenborn, A.M. (1994). The high-resolution three-dimensional solution structures of the oxidized and reduced states of human thioredoxin. *Structure* 2, 503–522.
36. Qin, J., Clore, G.M., Kennedy, W.P., Huth, J.R. & Gronenborn, A.M. (1994). Solution structure of human thioredoxin in a mixed disulfide intermediate complex with its target peptide from the transcription factor NFκB. *Structure* 3, 289–297.
37. Ren, X., Bjornstedt, M., Shen, B., Ericson, M.L. & Holmgren, A. (1993). Mutagenesis of structural half-cystine residues in human thioredoxin and effects on the regulation of activity by selenodiglutathione. *Biochemistry* 32, 9701–9708.
38. Wollman, E.E., *et al.*, & Fradelizi, D. (1988). Cloning and expression of a cDNA for human thioredoxin. *J. Biol. Chem.* 263, 15506–15512.
39. Tonissen, K.F. & Wells, J.R. (1991). Isolation and characterization of human thioredoxin-encoding genes. *Gene* 102, 221–228.
40. Kaghad, M., Dessarps, F., Jacquemin-Sablon, H., Caput, D., Fradelizi, D. & Wollman, E.E. (1994). Genomic cloning of human thioredoxin-encoding gene: mapping of the transcription start point and analysis of the promoter. *Gene* 140, 273–278.
41. Jeng, M.-F., Holmgren, A. & Dyson, H.J. (1995). Proton sharing between cysteine thiols in *Escherichia coli* thioredoxin: implications for the mechanism of protein disulfide reduction. *Biochemistry* 34, 10101–10105.
42. Ingelman, M., Nordlund, P. & Eklund, H. (1995). The structure of a reduced mutant T4 glutaredoxin. *FEBS Lett.* 370, 209–211.
43. Forman-Kay, J.D., Clore, G.M., Wingfield, P.T. & Gronenborn, A.M. (1991). High-resolution three-dimensional structure of reduced recombinant human thioredoxin in solution. *Biochemistry* 30, 2685–2698.
44. Johnson, R.S., Mathews, W.R., Biemann, K. & Hopper, S. (1988). Amino acid sequence of thioredoxin isolated from rabbit bone marrow determined by tandem mass spectrometry. *J. Biol. Chem.* 263, 9589–9597.
45. Rimsky, L., *et al.*, & Bertoglio, J. (1986). Purification to homogeneity and NH_2-terminal amino acid sequence of a novel interleukin 1 species derived from a human B cell line. *J. Immunol.* 136, 3304–3310.
46. Holmgren, A. (1977). Bovine thioredoxin system. *J. Biol. Chem.* 252, 4600–4606.
47. Eggleston, D.S. & Hodgson, D.J. (1982). Conformation and structure of acidic dipeptides. *Int. J. Pept. Prot. Res.* 19, 206–211.
48. Dyson, H.J., Tennant, L.L. & Holmgren, A. (1991). Proton-transfer effects in the active-site region of *Escherichia coli* thioredoxin using two-dimensional ^{1}H NMR. *Biochemistry* 30, 4262–4268.
49. Langsetmo, K., Fuchs, J.A. & Woodward, C. (1991). The conserved, buried aspartic acid in oxidized *Escherichia coli* thioredoxin has a pK_a of 7.5. Its titration produces a related shift in global stability. *Biochemistry* 30, 7603–7609.
50. Tonissen, K., Wells, J., Cock, I., Perkins, A., Orozco, C. & Clarke, F. (1993). Site-directed mutagenesis of human thioredoxin. Identification of cysteine 74 as critical to its function in the "early pregnancy factor" system. *J. Biol. Chem.* 268, 22485–22489.
51. Holmgren, A. (1985). Thioredoxin. *Annu. Rev. Biochem.* 54, 237–271.
52. Holmgren, A. & Luthman, M. (1978). Tissue distribution and subcellular localization of bovine thioredoxin determined by radioimmunoassay. *Biochemistry* 17, 4071–4077.
53. Kallis, G.B. & Holmgren, A. (1980). Differential reactivity of the functional sulfhydryl groups of cysteine-32 and cysteine-35 present in the reduced form of thioredoxin from *Escherichia coli*. *J. Biol. Chem.* 255, 10261–10265.
54. Hol, W.G.J. (1985). The role of the α-helix dipole in protein function and structure. *Prog. Biophys. Mol. Biol.* 45, 149–195.
55. Kerr, K.A. & Ashmore, J.P. (1975). A neutron diffraction study of L-cysteine. *Acta Cryst. B* 31, 2022–2026.
56. Adman, E., Watenpaugh, K.D. & Jensen, L.H. (1975). NH–S hydrogen bonds in *Peptococcus aerogenes* ferredosin, *Clostridium pasteurianum rubredoxin* and *Chromatium* high potential iron protein. *Proc. Natl. Acad. Sci. USA* 72, 4854–4858.
57. Frazao, C., *et al.*, & Sheldrick, G.M. (1995). *Ab initio* determination of the crystal structure of cytochrome c_6 and comparison with plastocyanin. *Structure* 3, 1159–1169.
58. Dyson, H.J., Gippert, G.P., Case, D.A., Holmgren, A. & Wright, P.E. (1990). Three-dimensional solution structure of the reduced form of *Escherichia coli* thioredoxin determined by nuclear magnetic resonance spectroscopy. *Biochemistry* 29, 4129–4136.
59. Biquet, C., *et al.*, & Wakasugi, H. (1994). Thioredoxin increases the proliferation of human B-cell lines through a protein-kinase-C-dependent mechanism. *J. Biol. Chem.* 269, 28865–28870.
60. Oblong, J.E., Gasdaska, P.Y., Sherrill, K. & Powis, G. (1993). Purification of human thioredoxin reductase: properties and characterization by absorption and circular dichroism spectroscopy. *Biochemistry* 32, 7271–7277.
61. Messerschmidt, A. & Pflugrath, J.W. (1987). Crystal orientation and X-ray pattern prediction routines for area-detector diffractometer systems in macromolecular crystallography. *J. Appl. Cryst.* 20, 306–315.
62. Kabsch, W. (1988). Evaluation of single-crystal X-ray diffraction data from a position-sensitive detector. *J. Appl. Cryst.* 21, 916–934.
63. Weissman, L. (1982). Strategies for extracting isomorphous and anomalous signals. In *Computational Crystallography. (*Sayre, D., ed), pp. 56–63, Clarendon Press, Oxford, UK.
64. Holmgren, A. & Söderberg, B.-O. (1970). Crystallization and preliminary crystallographic data for thioredoxin from *Escherichia coli* B. *J. Mol. Biol.* 54, 387–390.
65. Brünger, A.T., Kuriyan, J. & Karplus, M. (1987). Crystallographic R-factor refinement by molecular dynamics. *Science* 235, 458–460.

66. Furey, W., Wang, B.C. & Sax, M. (1982). Crystallographic computing on an array processor. *J. App. Cryst.* **15**, 160–166.
67. Hendrickson, W. (1995). Stereochemically restrained refinement of macromolecular structures. *Methods Enzymol*. **115**, 252–270.
68. Laskowski, R.A., MacArthur, M.W., Moss, D.S. & Thornton, J.M. (1993). PROCHECK: a program to check the stereochemical quality of protein structures. *J. Appl. Cryst.* **26**, 283–291.
69. Insight II version 2.2.0, Biosym Technologies. (1993). San Diego, CA.
70. Nichols, A., Bharadwaj, R. & Honig, B. (1993). GRASP – graphical representation and analysis of surface properties. *Biophys. J.* **64**, A166.
71. Jones, A. (1978). A graphics model building and refinement system for macromolecules. *J. Appl. Cryst.* **11**, 268–272.
72. Pflugrath, J.W., Saper, M.A. & Quiocho, F.A. (1984). New generation graphics system for macromolecular modeling. In *Methods and Applications in Crystallographic Computing.* (Hall, S. & Ashida, T., eds), pp. 404–407, Clarendon Press, Oxford, UK.
73. Collaborative Computational Project, Number 4. (1994). The CCP4 suite: programs for protein crystallography. *Acta Cryst. D* **50**, 760–763.
74. GCG version 7. (1991). Genetics Computer Group, Madison, WI.
75. Kraulis, P.J. (1991). MOLSCRIPT: a program to produce both detailed and schematic plots of protein structures. *J. Appl. Cryst.* **24**, 946–950.
76. An, G. & Wu, R. (1992). Thioredoxin gene expression is transcriptionally up-regulated by retinol in monkey conducting airway epithelial cells. *Biochem. Biophys. Res. Commun.* **183**, 170–175.
77. Droogmans, L., Cleuter, Y., Wollman, E.E., Kettmann, R. & Burney, A. (1994). Nucleotide sequence of ovine thioredoxin cDNA. *DNA Seq.* **4**, 277–279.
78. Tonissen, K.F., Robins, A.J. & Wells, J.R.E. (1989). Nucleotide sequence of a cDNA encoding rat thioredoxin. *Nucleic Acids Res.* **17**, 3973.
79. Jones, S.W. & Luk, K.-C. (1988). Isolation of a chicken thioredoxin cDNA clone. *J. Biol. Chem.* **263**, 9607–9611.